Special issue of the 3rd International Conference on Computational and Experimental Science and Engineering (ICCESEN 2016)

Preparation, Characterization and Catalytic Properties of SBA-15-SO_3H Supported Tungstophosphoric Acid for Esterification Reaction

B. Erdem[a,*], S. Erdem[b], A. Çitak[c], C. Yavru[d] and R.M. Öksüzoğlu[d]

[a]Uludag University, Chemistry Department, Bursa, Turkey

[b]Uludag University, Physics Department, Bursa, Turkey

[c]Eskişehir Osmangazi University, Chemical Engineering Department, Eskisehir, Turkey

[d]Anadolu University, Material Science and Engineering Department, Eskisehir, Turkey

SBA-15-SO_3H supported tungstophosphoric acid (TPA, $H_3PW_{12}O_{40}$) mesoporous materials were synthesized by impregnation of TPA into the hydrothermally synthesized SBA-15-SO_3H and the catalytic performances were compared for the esterification reaction. The physical and chemical properties of the catalysts were characterized by XRD, SEM/EDX, FT-IR and N_2 adsorption/desorption techniques. The characterization results show that TPA/SBA-15-SO_3H retained the typical mesoporous structure of SBA-15-SO_3H. The experimental results indicated that TPA/SBA-15-SO_3H is a more efficient catalyst than SBA-15-SO_3H for the esterification reaction. The higher activity of TPA/SBA-15-SO_3H compared with that of SBA-15-SO_3H was consistent with the material having the low pKa value, confirming that the esterification rate was mostly dependent on the acid strength of the additional functional groups of solid acid catalyst. Accordingly, the reason for the catalytic activity difference was simply explicated by the effect of TPA, having low pKa value, affecting the pore structure and the total acidity.

DOI: 10.12693/APhysPolA.132.1041

PACS/topics: 61.43.Gt, 82.65.+r

1. Introduction

TPA is an important solid acid catalyst among the heteropoly acids, since it has superior properties, such as Brønsted acidity, structural interchangeability, high proton mobility and eco-friendliness [1]. Due to its structural features, TPA has been frequently used as an efficient catalyst for various organic reactions [2–6]. However, TPA has such deficiencies, as extremely low surface area ($< 10\ m^2\,g^{-1}$), porous structure and thermal stability, which result in the limited usage of it in various acid catalyzed reactions [7]. Therefore, it is being used after impregnation onto various carriers, such as silica, active carbon, molecular sieves, Al_2O_3 and so on [1].

The surface modification of mesoporous silica, like SBA-15, using organosilane compound has opened up new possibilities of controlling not only the acid strength, but also the number of sites [8]. However, the catalytic activity of sulfonic acid functionalized SBA-15, named as SBA-15-SO_3H is not very high, compared to homogeneous strong acid catalyst. Thus, impregnation of TPA on SBA-15-SO_3H, with its combination of high surface area, large pore diameter, and high pore volume, is seen as a critical heterogeneous catalytic application.

In this study, we aimed to improve the catalytic activity of SBA-15-SO_3H by impregnating TPA onto the sulfonic acid functionalized mesoporous silica SBA-15-SO_3H and to test the performance of this material (TPA/SBA-15-SO_3H) in the esterification of propionic acid with methanol.

*corresponding author; e-mail: gbeyhan@uludag.edu.tr

2. Experimental

2.1. Synthesis of TPA/SBA-15-SO_3H

Sulfonic acid functionalized mesoporous silica (SBA-15-SO_3H) was synthesized by using one-pot method, as described in the literature [9–12]. In a typical synthesis, 4 g of Pluronic P123 triblock copolymer was diluted in the acidic medium until a clear solution was obtained. 7.69 g of TEOS, used as silica source, was added and stirred at 40 °C for pre-hydrolysis. 0.81 g of 3-mercaptopropyl trimethoxysilane and 8.37 g of H_2O_2 were added, then the resulting mixture was stirred for 21 h at 40 °C, followed by aging at 100 °C for another 21 h under static conditions. To remove the template, extraction with ethanol under reflux for 24 h was realized.

To prepare TPA incorporated SBA-15-SO_3H samples, 1 g of SBA-15-SO_3H was impregnated with an aqueous solution of TPA (0.05 g/10 ml and 0.1 g/10 ml) and dried at 100 °C for 10 h. The samples were labeled as TPA_1/SBA-15-SO_3H, TPA_2/SBA-15-SO_3H. The loading amount of TPA was calculated by the following equation.

$$\text{Loading amount}(\%) = \frac{m_{\text{TPA}}}{m_{\text{TPA}} + (m_{\text{SBA-15-SO}_3\text{H}})} \times 100, \quad (1)$$

were m_{TPA} is weight of TPA and $m_{\text{SBA-15-SO}_3\text{H}}$ is weight of SBA-15-SO_3H. For the series of catalysts, TPA_1/SBA-15-SO_3H and TPA_2/SBA-15-SO_3H,

the subscripts 1 and 2 indicate loading of TPA, which is 5% and 10%, respectively, according to the given formula.

2.2. Characterization

X-ray powder diffraction patterns were collected on a Bruker D8 Advance diffractometer using Cu-K_α radiation for low (0.5° to 3°) and high (10° to 60°) 2θ angles of XRD, respectively.

The elemental analysis of the samples was studied using energy-dispersed X-ray spectra (EDX-Quanta-Bruker AXS). A Thermo Nicolet 6700 series infrared spectrometer was used for FT-IR analysis in normal transmission mode with a KBr detector, over the range of 4000–400 cm^{-1} at a resolution of 8 cm^{-1}, averaged over 32 scans. Nitrogen sorption isotherms were measured at 77 K with Quantachrome, Autosorb 1C sorption analyzer. Before the measurements, the samples were degassed at 200 °C in vacuum for 5 h. Surface areas were calculated using the Brunauer-Emmet-Teller (BET) method over the range of $P/P_0 = 0.03 - 0.2$, where a linear relationship is maintained. Pore size distributions were calculated using the Barrett-Joyner-Halenda (BJH) model, applied to the desorption branch of the isotherm.

2.3. Catalytic reaction

Stoichiometric ratio of propionic acid to methanol was (1:3) in the experiments performed at 333 K. 1,4-dioxane was used as solvent in all experiments. Samples, withdrawn at regular time intervals, were analyzed by titration with 0.1 M sodium hydroxide. Propionic acid conversion versus time was calculated according to Eq. (2) where C_{A0} and C_A represent the propionic acid concentration in initial state and after t minutes, respectively.

$$X_A = \frac{C_{A0} - C_A}{C_{A0}}. \tag{2}$$

3. Results and discussion

The X-ray diffractograms of pure SBA-15-SO_3H and TPA/SBA-15-SO_3H samples at low and high-Bragg angles are shown in Fig. 1a and b, respectively. All of the samples show three main peaks, matching well with the characteristic patterns of the well-ordered mesoporous silica. Even if the intensities of these peaks decrease for TPA/SBA-15-SO_3H samples, which indicates the deposition of TPA within the mesopores, causing the deformations in the ordered structure of the pores, SBA-15-SO_3H still keeps its mesoporous structure because of the low TPA loading.

In Fig. 1b, a broad peak around 24°, which was observed for all samples, is corresponding to the amorphous structure of silica [13]. On the other hand, no characteristic peaks of bulk crystal TPA appear in TPA/SBA-15-SO_3H materials, indicating the high dispersion of TPA on the surface of amorphous pore walls of SBA-15-SO_3H [2].

EDX analysis shows that TPA was incorporated into the SBA-15-SO_3H sample (Fig. 2). This situation is due

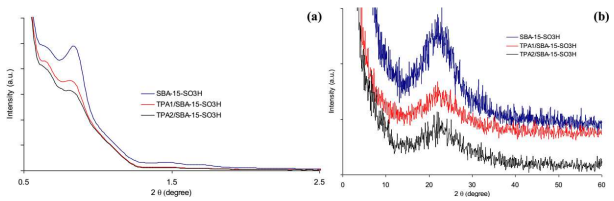

Fig. 1. Low angle (a) and high angle (b) XRD patterns of SBA-15-SO_3H and TPA/SBA-15-SO_3H samples.

to the large mesopores of SBA-15-SO_3H, which allows TPA to pass into the pores of the material. This result is consistent with the N_2 adsorption/desorption result [14]. Consequently, TPA could penetrate into the mesopores of SBA-15-SO_3H.

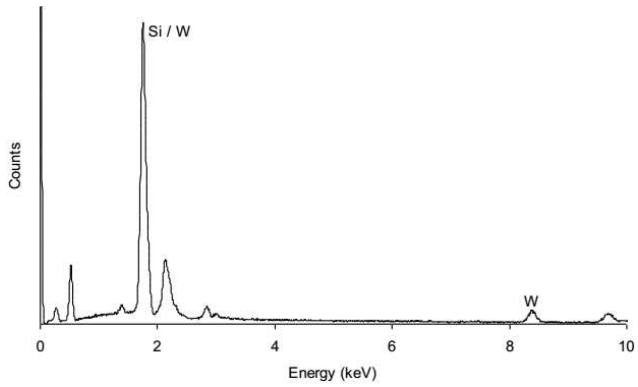

Fig. 2. EDX spectrum of TPA_2/SBA-15-SO_3H.

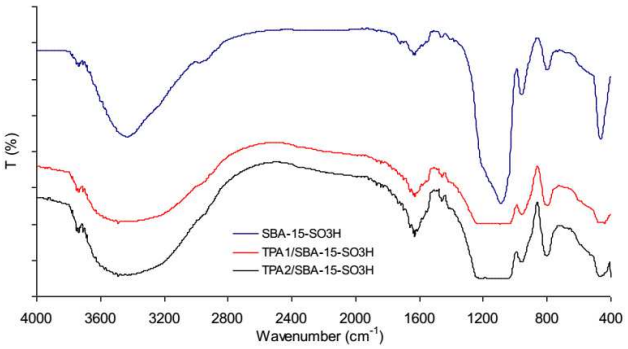

Fig. 3. FT-IR spectra of SBA-15-SO_3H, TPA_1/SBA-15-SO_3H and TPA_2/SBA-15-SO_3H.

The characteristic absorption peaks of mesoporous silica (Fig. 3) are evident at 450 cm^{-1} (SiO_4), 800 cm^{-1} (Si–O–Si), 960 cm^{-1} (Si–O), and a large band between 1000 and 1260 cm^{-1} (Si–O–Si) vibrations. In addition, the band at 1450 cm^{-1} can be assigned to the C–CH_2–C vibrational mode, the band at 2850–2900 cm^{-1} is clearly observed as the C–H vibrations.

FT-IR spectra of TPA/SBA-15-SO_3H were almost the same as those of the SBA-15-SO_3H, except for the band around at 800 cm^{-1}, which increased with the increase of TPA loading amount, indicating the incorporation

of TPA into the SBA-15-SO_3H, and for the band at 960 cm^{-1}, which decreased with the increase of TPA loading amount, indicating that TPA was attached to the structure by means of free silanol groups.

The absorption peaks of TPA around 1082 (P–O band) and 980 cm^{-1} (W=O band) can not be observed, owing to the overlapping of TPA bands with those of SBA-15-SO_3H [15]. In addition, as the TPA loading increases, the peaks at 1637 and 3450 cm^{-1} become broader. These bands are ascribed to the bending and stretching vibrations of bridging hydroxyl, because of the interaction of TPA and surface silanol groups of SBA-15-SO_3H [5].

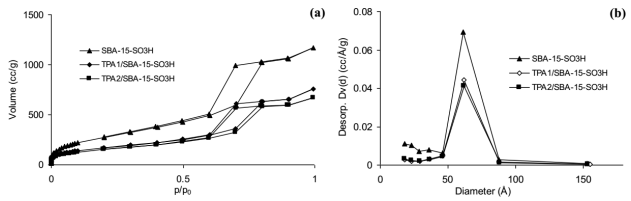

Fig. 4. N_2 adsorption/desorption isotherms (a) and pore size distributions (b) of SBA-15-SO_3H, TPA_1/SBA-15-SO_3H and TPA_2/SBA-15-SO_3H.

All N_2 adsorption/desorption isotherms (Fig. 4a) are of the type IV, according to the IUPAC classification and exhibited an H1 hysteresis loop, which is a characteristic of mesoporous solids. The adsorption branch of each isotherm showed a sharp inflection, which means a typical capillary condensation within uniform pores and considerable adsorption amounts indicate that there is a considerable volume of nanospaces, even after the introduction of TPA. In addition, narrow pore size distribution was observed (Fig. 4b) for all samples, indicating long range order [5].

According to Table I, as the TPA loading increases, the surface area and pore volume strongly decrease while pore sizes of the samples do not change dramatically. This situation might be caused by the fact that TPA molecules were distributed all over the external surface of the silicate structure and blocked the pores [13]. Narrow pore size distribution curve, the high BET surface area, mean pore size and pore volume, plus the distinct X-ray reflection peaks demonstrate that the TPA/SBA-15-SO_3H has a hexagonal mesoporous structure, as observed in the literature [16, 17].

TABLE I

Textural and acidic properties of pure and TPA anchored SBA-15-SO_3H.

Samples	Surface area [m^2/g]	Pore volume [cm^3/g]	Pore size [nm]	Acid capacity [meq/g]
SBA-15-SO_3H	1012	1.638	7.145	0.5273
TPA_1/SBA-15-SO_3H	618.9	1.169	7.556	0.5429
TPA_2/SBA-15-SO_3H	559.8	1.035	7.393	0.6584

As can be seen in Table I, SBA-15-SO_3H has an acid site because of having sulfonic acid functional group the pKa value of which is 1.89. When TPA (pKa: 1.60) was anchored to SBA-15-SO_3H, acid site increases because of having lower pKa value compared to sulfonic acid. As TPA loading increases, acidity values also increase and the results are as expected. It is clearly observed from Fig. 5 that with the increase in the loading of TPA, conversion X_A also increases.

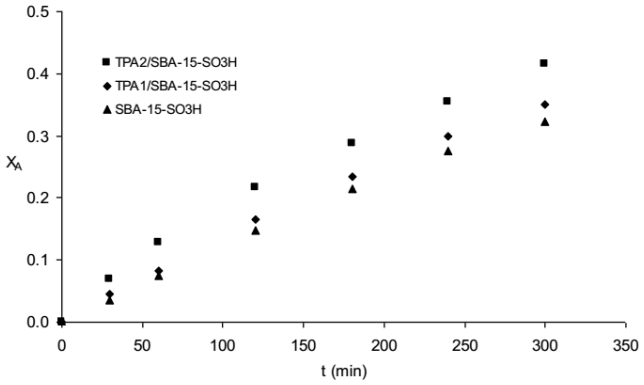

Fig. 5. Propionic acid conversions for SBA-15-SO_3H, TPA_1/SBA-15-SO_3H and TPA_2/SBA-15-SO_3H.

The lower pKa value for TPA additional functional group was consistent with the enhanced acid strength and reaction conversion of the acid catalyst through a cooperative effect, due to the proximity of acidic groups. The mutual interaction between the acid sites increased for increasing surface concentration, due to the formation of hydrogen bonds between adjacent acid sites, leading to a higher overall acid strength of the solid catalyst [18].

4. Conclusions

TPA was successfully anchored to the SBA-15-SO_3H acid catalyst, which was evaluated in the methyl alcohol propionic acid esterification. As the TPA loading increased, the surface area and pore volume of the TPA/SBA-15-SO_3H samples decreased. On the other hand, the acidity was enhanced by increasing the loading of TPA. The higher activity of TPA/SBA-15-SO_3H, compared with that of SBA-15-SO_3H, was consistent with the material having the lower pKa value, confirming that the esterification of methanol with propionic acid was mostly dependent on the acid strength of the additional functional groups of solid acid catalyst.

References

[1] S. Wu, J. Wang, W. Zhang, X. Ren, *Catalysis Lett.* **125**, 308 (2008).

[2] Q.Y. Liu, W.L. Wu, J. Wang, X.Q. Ren, Y.R. Wang, *Microporous Mesoporous Mater.* **76**, 51 (2004).

[3] N.Y. He, C.S. Woo, H.G. Kim, H.I. Lee, *Appl. Catal. A* **281**, 167 (2005).

[4] V. Brahmkhatri, A. Patel, *Industrial Engin. Chem. Res.* **50**, 6620 (2011).

[5] V. Brahmkhatri, A. Patel, *Appl. Catal. A* **403**, 161 (2011).

[6] A. Sakthivel, K. Komura, Y. Sugi, *Industrial Engin. Chem. Res.* **47**, 2538 (2008).

[7] D.P. Sawant, J. Justus, V.V. Balasubramanian, K. Ariga, P. Srinivasu, S. Velmathi, S.B. Halligudi, A. Vinu, *Chem. Europ. J.* **14**, 3200 (2008).

[8] J.K. Shon, X. Yuan, C.H. Ko, H.I. Lee, S.S. Thakur, M. Kang, M.S. Kang, D. Li, J.N. Kim, J.M. Kim, *J. Industrial Engin. Chem.* **13**, 1201 (2007).

[9] X. Liu, F. Chang, L. Xu, Y. Yang, P. Tian, L. Qu, Z. Liu, *Microporous Mesoporous Mater.* **79**, 269 (2005).

[10] Y. Zheng, J. Li, N. Zhao, W. Wei, Y. Sun, *Microporous Mesoporous Mater.* **92**, 195 (2006).

[11] S. Miao, B.H. Shanks, *Appl. Catal. A* **359**, 113 (2009).

[12] A. Çıtak, B. Erdem, S. Erdem, R.M. Öksüzoğlu, *J. Colloid Interface Sci.* **369**, 160 (2012).

[13] B. Aydemir, N.A. Sezgi, T. Doğu, *AIChE J.* **58**, 2466 (2012).

[14] Z. Obalı, N.A. Sezgi, T. Doğu, *Chem. Engin. Communicat.* **196**, 116 (2009).

[15] Y. Xu, Y. Qi, G. Lu, S. Li, *Catalysis Lett.* **125**, 83 (2008).

[16] H.Y. Wu, X.L. Zhang, X. Chen, Y. Chen, X.C. Zheng, *J. Solid State Chem.* **211**, 51 (2014).

[17] Y. Ha, Y. Li, *J. Porous Mater.* **22**, 721 (2015).

[18] I.K. Mbaraka, B.H. Shanks, *J. Catalysis* **244**, 78 (2006).